Original Paper

Landslides
DOI 10.1007/s10346-024-02375-w
Received: 25 May 2023
Accepted: 17 September 2024

J. M. Kimball · E. T. Bowman · J. M. N. T. Gray · W. A. Take

Evaluation of laboratory methods to quantify particle size segregation using image analysis in landslide flume tests

Abstract Landslides comprised of a wide range of particle sizes (e.g. debris flows) exhibit flow structures arising from particle size segregation. Segregation influences the mobility of the flow, the development of debris fans, and the resulting impact forces to be expected when designing barriers and containment structures. In order to capture the flow dynamics of segregable materials in numerical simulations, experimental datasets quantifying segregation in the final deposit are required. However, the measurement of segregation is not a straightforward task as segregation observed at an external transparent boundary may not be indicative of segregation within the bulk of the landslide mass due to sidewall friction. In this paper, we explore the use of four different strategies to optically measure particle size segregation in large landslide flume tests, comparing measurements taken (i) at the external transparent flume boundary; (ii) using a thin transparent plane as a splitter plate along the centre of the flow; and using a (iii) vertically or (iv) horizontally inserted transparent plate into the static deposit after flow arrest. Relationships between concentrations measured by projected area (i.e. sidewall image) to concentrations by mass are derived and validated for a tridisperse mixture to assess which sampling method most closely represented the original source volume. Of the four strategies tested, the transparent splitter plane method was identified to cause the least amount of out-of-plane segregation of particles, provides a rich database of highly detailed observations of segregation of tridisperse granular flows that can be used to evaluate future numerical model outcomes, and is recommended for future laboratory flume investigations.

Keywords Segregation · Landslides · Image analysis · Flume experiments

Introduction

Particle size segregation is a phenomenon observed in granular flows of mixed particle sizes resulting in preferential sorting longitudinally and vertically within the flow. In a geohazards context, this means that landslides which exhibit a large range of particle sizes, such as debris flows, are characterized by flow structures arising from significant particle size segregation. Vertical segregation is controlled by two primary mechanisms: particle percolation, which is the effect of small particles falling into voids towards the flow base, and squeeze expulsion, which describes the upwards squeezing of all particle sizes during shear (Savage and Lun 1988). These combined processes result in the development of upwards coarse grading granular flow structures. Furthermore, this preferential vertical sorting of large particles towards the surface of the flow has implications for longitudinal sorting as the surface velocity is typically the fastest portion of the flow velocity profile. This effect leads to preferential transport of large particle sizes to the front of the flow. In the context of a debris flow, longitudinal sorting results in a dry coarse-grained flow front, followed by a transition zone and then a finer-grained flow tail (Fig. 1). The phenomenon of particle size segregation is therefore a key process defining the behaviour of polydisperse granular flows and will significantly influence its mobility, the development of debris fans, or resulting impact forces on structures.

Considerable advances in both physical modelling as well as theoretical and numerical models of granular flow segregation have been reported in the literature (Gray 2018). The majority of theoretical models focus on segregation in bi-dispersed granular mixtures (e.g. Fan et al. 2014; Gray and Chugunov 2006; Gray and Thornton 2005; Savage and Lun 1988) with few describing the more complex process of segregation in multi-component (Gray and Ancey 2011; Deng et al. 2018) or polydisperse mixtures (Schlick et al. 2016; Barker et al. 2021). Numerical simulations using methods such as the discrete element method (DEM) or discrete particle method (DPM) have been employed to model segregation in granular flows. These models have been shown to produce accurate results through comparison with experimental datasets and subsequent model calibration (e.g. Jiang et al. 2018; Jing et al. 2018; Ming Cheng et al. 2019; Wiederseiner et al. 2011; Cúñez et al. 2024). Most of these studies investigate the process of segregation during steady state flow pertinent to industrial processes. In contrast, landslides exhibit an initial acceleration phase of confined or unconfined flow over variably inclined terrain before eventually coming to rest as a static deposit.

Validation of numerical simulations of segregation of geophysical flows would ideally be based on the segregation observed in such a deposit. However, experimental quantification of particle size segregation is difficult, as boundary measurements taken through a transparent window may not be fully representative of the internal structure. This challenge is illustrated visually in Fig. 2. Visual observations at an external window (Fig. 2a) are subject to bias due to sidewall influence. In contrast, internal measurements (Fig. 2b) require the generation of a deposit cross section in a manner which minimizes deposit disturbance. Refractively matched index experiments, which utilized transparent media, have been used to study both granular flows and specifically particle size segregation processes (van der Vaart et al. 2015, 2018; Sanvitale and Bowman 2016, 2017; Trewhela et al. 2021). These types of experiments allow for undisturbed observation of internal flow and/or segregation processes. Similarly, X-ray computed tomography (CT) has been used to observe undisturbed three-dimensional complex motion dynamics arising from particle size segregation (Gajjar et al. 2021).

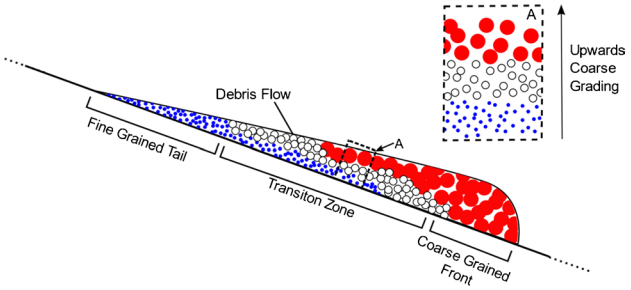

Fig. 1 Schematic illustrating material flow down an incline, highlighting flow body morphology and particle size segregation longitudinally across the body and vertically in the form of upwards coarse grading of body material

However, such experiments are currently limited in scale. Another method used to observe internal mechanisms of granular flows was carried out by Kokelaar et al. (2014). Deposits of small-scale size segregating flows were impregnated with a low-viscosity acrylic resin, sectioned, and polished for examination. Although effective for small-scale purposes, this method is not practical for use in large-scale experiments. In small-scale experiments, Viroulet et al. (2018) used a splitter plate placed part way down and along the centerline of a small-scale flume, parallel to the flume sidewalls and perpendicular to the flume base, to observe interior flow dynamics. However, the extent of bias generated in these flows due to particle interaction with the splitter plate is unclear. Currently, for large-scale experiments, the most practical approach to obtain internal deposit information requires an incision into the deposit, similar in concept to that completed by Viroulet et al. (2018), which potentially introduces a sampling method bias.

Possible options for generating this incision and a resulting visible internal cross section include securing a transparent plane along the centerline of a runout zone prior to material deposition (Fig. 2c) inserting a transparent plane into the deposited material in the horizontal direction (Fig. 2d) in the horizontal direction in increments (Fig. 2e) or vertical direction (Fig. 2f). The magnitude to which the measurement and quantification of particle size segregation will be influenced by the sampling method is currently unclear.

The objective of this paper is to quantitatively assess four different strategies to optically measure particle size segregation in flume tests, comparing measurements taken (i) at the external transparent flume boundary; (ii) using a thin transparent plane as a splitter plate along the centre of the flow; and using a (iii) vertically or (iv) horizontally inserted transparent plate into the static deposit following flow arrest. Relationships between concentrations measured by projected area (i.e. sidewall image) to concentrations by mass will be derived and validated for the tridisperse mixture in order to assess which sampling method most closely represents the known concentration of the source volume. This measure will therefore enable the quantification of the degree to which each measurement strategy causes out-of-plane segregation of particles observed in large-scale flume experiments. In doing so, the work aims to create a database of highly detailed observations of quantification of vertical and longitudinal segregation of a tridisperse granular flow that can be used to evaluate future numerical model outcomes.

Materials and methods

Queen's landslide flume

The Queen's University landslide flume facility consists of a landslide source volume retained in a release box above a 30° inclined slope and a subsequent horizontal runout section (e.g. Bullard et al. 2019a, 2019b, 2023; Taylor-Noonan et al. 2022). Key to the quantification of segregation using image analysis, the flume is equipped with transparent sidewalls and a mechanism developed in the present study to permit the insertion of a transparent plane into the deposit to create an internal transparent cross-section (Fig. 3). Details for each of these flume components are described in detail in the following sections.

The flume structure is a 2.1 m wide, 6.73 m long, channel inclined at a slope of 30°. The sides of the flume consist of 19 mm thick and 1.21 m tall tempered glass panes and an aluminum flume base over the inclined section and first 3.66 m of the horizontal runout section of the flume. Beyond this, the flume walls and base transition to concrete for an additional 29.34 m. In the present study, the maximum travel distance along the base of the flume in all experiments is less than 3.66 m, resulting in the aluminum interface basal friction conditions representing the boundary conditions for the full duration of each flow.

The 0.6 m^3 landslide source volume consists of tridisperse particles (3 mm, 6 mm, and 12 mm nominal diameter) in a pre-mixed state behind a rotating release door. The initial mixture was achieved by shoveling the material into a heap, mixing by shovel, and into buckets for delivery to the release box. These buckets were then lifted to the elevated release box via an PRO400 Platform Hoist in mixed batches of approximately 0.045 m^3. For each lift, the material was leveled to ensure a uniform distribution of particle sizes, slowly building a source volume in the shape of a triangular prism (Fig. 3). This volume was then released down the flume by opening the release box door.

A Phantom v2512 high-speed camera, equipped with a Tokina 100 mm f/8 macro lens, was placed at the bottom of the inclined section of flume (CAM1 in Fig. 3), to capture particle scale interactions along the flume incline. The widest aperture was used on the lens to capture the movement of particles closest to the flume sidewall. Greyscale images were taken at a rate of 7500 fps, at a resolution of 1280 × 800 pixels, with a field of view measuring approximately 220 mm × 136 mm. At this scale factor, particle diameters observed ranged between 15 pixels (3 mm particles) and 75 pixels (12 mm particles) in the acquired images.

After the mixture came to rest, the static deposit was imaged along the sidewall to capture the entire length of the deposit in 0.1 m increments using a Sony DSC-RX10 II camera at a resolution of 5472 × 3648 pixels and Neewer Dimmable LED lights. These images captured an external view of the deposit morphology and particle size distribution. Particle diameter in pixels varied typically between 30 pixels (3 mm particles) and 150 pixels (12 mm particles) in these sidewall images.

A mechanism was developed in the presented study to permit the insertion of a thin transparent plane into the deposit to create an internal transparent cross-section. A 6.25 mm thick, 0.4 m × 2.44 m tempered glass pane fitted with a 50 mm long leading aluminum cutting wedge was selected to minimize sample disturbance but still maintain structural integrity during the installation process. An articulated support system was used to place and secure the pane in a fixed plane along the centerline

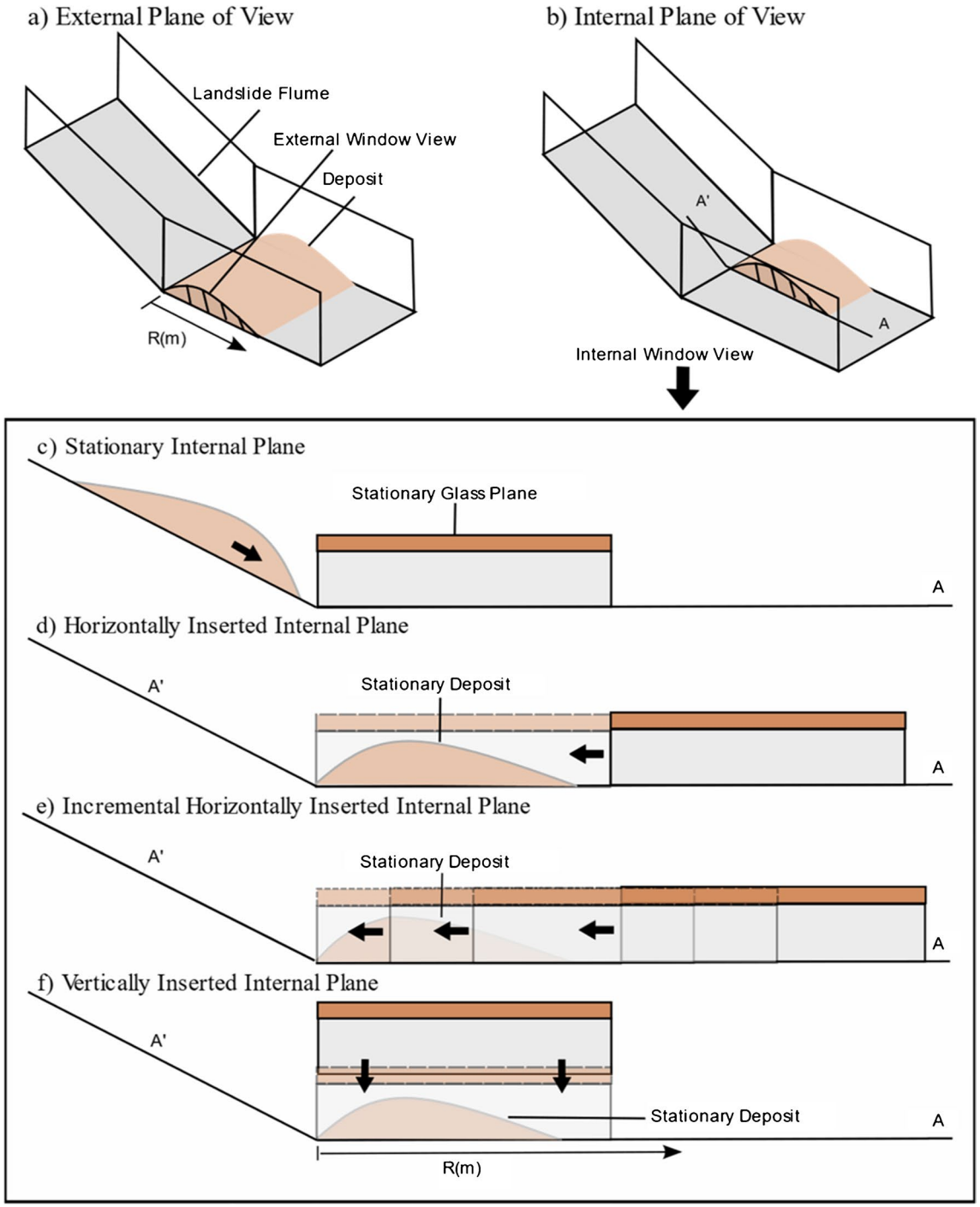

Fig. 2 Landslide deposit observation points at **a** an external flume window and **b** a cross-section created inside the landslide deposit using a thin, 6.35 mm thick, tempered glass plane to section the deposit by **c** being stationary and present in the runout area, **d** being horizontally inserted into the stationary deposit, **e** being horizontally inserted into the stationary deposit in increments, and **f** being vertically inserted into the stationary deposit

of the flume for internal deposit observation. Material deposited on one side of the transparent plane was removed to make the material on the other side of the transparent plane visible for observation. This transparent plane, now exposing internal deposit morphology, was then imaged in the same manner as the flume sidewall.

Several internal deposit sampling methods were trialled as shown in Fig. 2. For the stationary internal plane method (Fig. 2c), the internal plane was secured along the centerline of the flume prior to the material release. The horizontally inserted plane method involved sliding the internal plane into the deposit from the front continuously until the full deposit was sectioned. The incremental horizontally

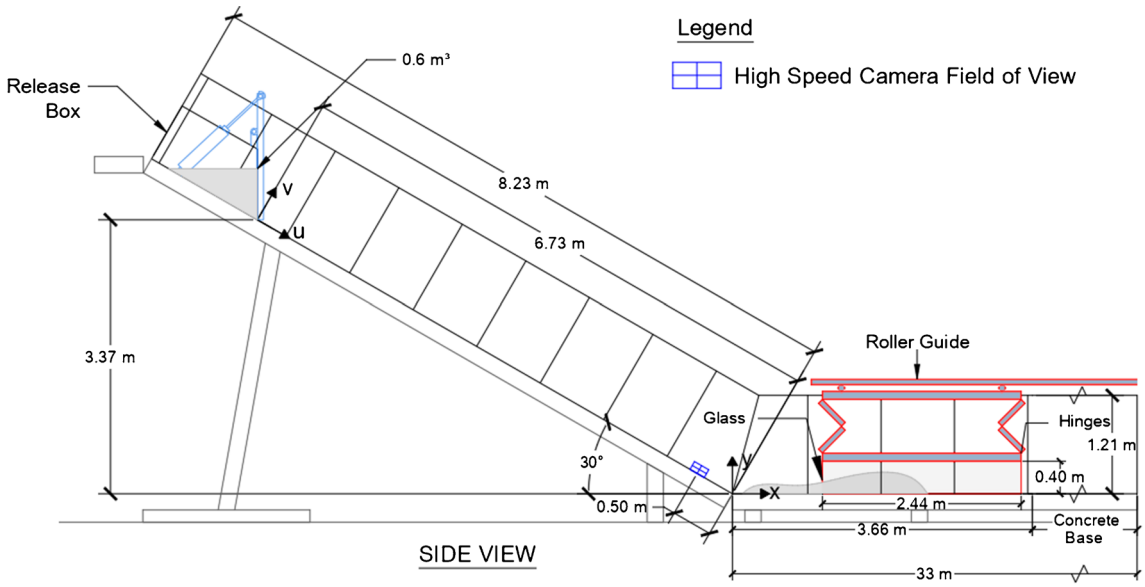

Fig. 3 Schematic of the Queen's landslide flume and articulated support system for thin, 6.35 mm thick, plane of tempered glass used for deposit sectioning

inserted internal plane method (Fig. 2d) involved sliding the internal plane into the deposit from the front in increments to minimize the shearing effect. In detail, the plane was initially inserted 0.5 m so that the most distal 0.3 m of deposit could be imaged after excavation in front, then further inserted in 0.3 m increments until the whole deposit was examined (allowing the 0.2 m closest to the undisturbed deposit to remain intact each time). The vertical insertion of a plane (Fig. 2f) was unsuccessful as the plane was unable to reach the base of the flume in a consistent and controlled manner. For this reason, this method was not further investigated.

Materials

Commercially available ceramic particles, marketed as Denstone 2000 Support Media and manufactured by Saint-Gobain Norpro, were used to create the tridisperse mixture source volume. An even mixture by mass of 3 mm, 6 mm, and 12 mm nominal diameter particles was chosen to simplify the interpretation of data by ensuring each component of the mixture was present in equal proportions. These particular particles were selected for their resistance to fracture, similar density to typical geophysical flow materials (2200 kg/m^3), their pseudo-spherical shape (92–96% sphericity, to avoid rolling friction associated with perfectly spherical particles), and uniformity of particle size (diameters of 3.85 ± 0.41 mm, 7.03 ± 0.38 mm, and 13.43 ± 0.66 mm, respectively) as measured by Coombs et al. (2020).

Image analysis techniques for quantifying landslide thickness and velocity

A key aspect of the experimental design was to examine the repeatability of the landslide experiment. Image analysis techniques were therefore used to characterize the velocity and flow height of the replicate landslide experiments through high-speed camera data collection. Flow height data was obtained by taking frames every 0.05 s of flow and manually tagging the top of flow in each frame. Velocity data was obtained using particle tracking velocimetry (PTV). PTV requires the identification of particle locations from successive frames to determine particle movement between frames. The particle-mask-correlation method (Takehara and Etoh 1999; Gollin et al. 2017; Taylor-Noonan et al. 2021) was used to identify particles from the high-speed camera frames. Masks were generated, using two-dimensional Gaussian distributions, to match the appearance of test particles. These masks were square in shape with the Gaussian distribution beginning at the center of the mask and extending radially in all directions for a distance of half the square width. This resulted in a circular Gaussian distribution surrounded by solid dark corners (Fig. 4b) which matched shadowing often present around the particles imaged. Masks were generated in a range of sizes via visual assessment to encompass the range present in the flow. Once a particle was identified, its location was calculated on a subpixel level by completing a least-squared-error fit between the subject frame and particle mask.

For this study, the cross-correlation method was used in a PTV algorithm to track the particles between images (Gollin et al. 2017). Velocity data was collected at intervals of 0.1 s of flow by averaging over ten consecutive frames over a time period of 1.33 ms. Velocity data were then binned to enable them to be separated by height. For each time interval, the top flow velocity values were taken from the vertical bin nearest in height to the identified flow height, while mean velocity values were taken as the mean of the velocities throughout the flow height, and the basal slip velocity was taken to be that of the bin closest to the flume base.

Development of image analysis methods to quantify segregation

Deposit imaging analysis

Optical quantification of the degree of segregation requires high-resolution images of the deposit to be taken throughout the entire

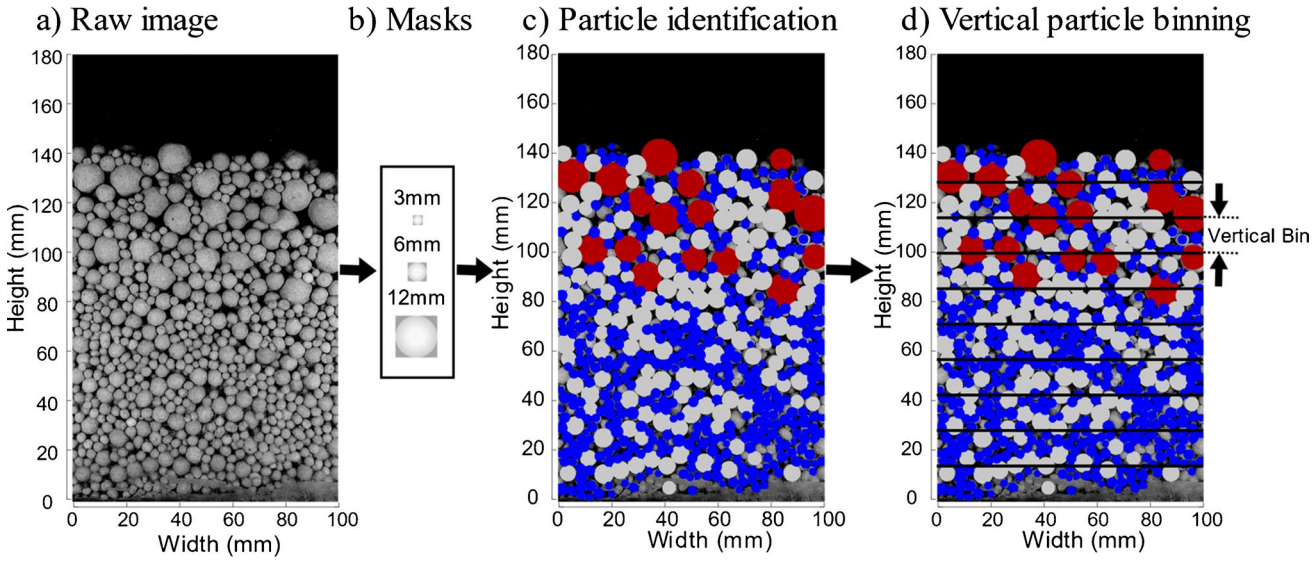

Fig. 4 Image analysis process starts with **a** a raw image, on which **b** the particle masks are correlated to the raw image, for **c** the identification of particles locations and sizes, and **d** the vertical binning of identified particles, for concentration by area calculations

profile of the static deposit. Images were captured every 0.1 m at a transparent boundary to analyze the distribution of particle sizes. The captured images were converted to greyscale and cropped such that the height of the image incorporated the base and top of the deposit and such that the width of the image generated a 0.1 m wide field of view (FOV) (Fig. 4a). The particle-mask-correlation method was used to identify particles and their positions within the images. Sample masks used are shown in Fig. 4b. Once particles were identified (Fig. 4c), the relative concentrations of each particle size based on area could be determined by dividing the area occupied by one particle size by the area occupied by all identified particles. Compiling the concentration results of the multiple images taken at various locations along the flume base allowed for the observation of longitudinal segregation in the deposits. Vertical segregation was also observed and analyzed using the same 0.1 m cropped images. This was done by generating 10 equally sized vertical bins (Fig. 4d), based on the local height of the deposit. The concentration of a particular particle size in each bin was calculated as above. If a particle was located along the boundary of a bin, the fraction of the particle area within the bin was used in the calculation.

Relationship between particle concentration by area and mass/solid volume

Images of particles captured at a vertical transparent boundary represent the projected area of the different particle sizes at the plane of the window. However, additional analyses are required to translate particle concentration based on area to particle concentration based on volume or mass (Diplas and Sutherland 1988; Bunte and Abt 2001; Graham et al. 2012). This is because the projected area of a spherical particle scales with the square of its radius, while its volume scales with its cube.

In the literature, empirically derived factors are used to develop conversion relationships between particle concentration by area and by solid volume or mass (Diplas and Sutherland 1988; Graham et al. 2012). Equation (1) presents a rewritten version of the equation by Cuttler et al. (2017):

$$V_{W_i} = \frac{A_{W_i} * D_i^X}{\Sigma A_{W_i} * D_i^X} \tag{1}$$

where V_{W_i}, is the volume by weight portion of the ith grain size, A_{W_i} is the area portion occupied by the ith particle size, D_i is the diameter of the ith particle size, and X is an empirically determined conversion factor. This conversion method is widely applicable to coarse particle size distributions with varying degrees of angularity.

Given the primary focus of the quantification of segregation in this work, a specific theoretical relationship is derived here between concentrations based on area and mass/solid volume for tridisperse mixtures. Coombs et al. (2020) found the subject 3, 6, and 12 mm particles had similar particle densities, 2241 kg/m^3, 2242 kg/m^3, and 2195 kg/m^3, respectively. Therefore, it is reasonably assumed that particle density, ρ, is independent of particle size. It is also assumed that particles are perfectly spherical. Hence, for each respective particle size, area (A) is calculated as $A = \pi r^2$, where r is the particle radius; volume (V) is calculated as $V = \frac{4}{3}\pi r^3$; and mass (M) is calculated as $M = \rho V$. Concentration of each respective particle size (i) in terms of mass is calculated as

$$C_{Mi} = \frac{M_i}{M_1 + M_2 + M_3} = \frac{\rho\left(\frac{4}{3}\pi r_i^3 n_i\right)}{\rho\left(\frac{4}{3}\pi r_1^3 n_1\right) + \rho\left(\frac{4}{3}\pi r_2^3 n_2\right) + \rho\left(\frac{4}{3}\pi r_3^3 n_3\right)} = \frac{r_i^3 n_i}{r_1^3 n_1 + r_2^3 n_2 + r_3^3 n_3} \tag{2}$$

Where C_{M_i} represents the concentration by mass of a particular particle size, and n_i represents the number of particles of that size present in a subject mixture. Concentration of each particle size in terms of area is calculated as.

$$C_{Ai} = \frac{A_i}{A_1 + A_2 + A_3} = \frac{\pi r_i^2 n_i}{\pi r_1^2 n_1 + \pi r_2^2 n_2 + \pi r_3^2 n_3} = \frac{r_i^2 n_i}{r_1^2 n_1 + r_2^2 n_2 + r_3^2 n_3} \tag{3}$$

The concentration by area of the three particle sizes is represented by the coefficients, C_{Ai}, with the assumption that $C_{A1} + C_{A2} + C_{A3} = 1$. The above equation rearranges to

$$r_i^2 n_i = C_{Ai}\left(r_1^2 n_1 + r_2^2 n_2 + r_3^2 n_3\right) and \frac{r_i^2 n_i}{C_{Ai}} = r_1^2 n_1 + r_2^2 n_2 + r_3^2 n_3 \tag{4a,b}$$

With the undefined coefficients isolated to equate to a common set of defined variables, the isolated coefficients can be defined for each particle size and equated:

$$\frac{r_1^2 n_1}{C_{A1}} = \frac{r_2^2 n_2}{C_{A2}} = \frac{r_3^2 n_3}{C_{A3}} \tag{5}$$

Which rearranges to

$$n_2 = \frac{r_1^2 n_1 C_{A2}}{C_{A1} r_2^2}; and n_3 = \frac{r_1^2 n_1 C_{A3}}{C_{A1} r_3^2} \tag{6a,b}$$

Equations (6a) and (6b) can be substituted into Eq. (2) and rearranged:

$$C_{M_1} = \frac{r_1^3}{r_1^3 + \frac{r_2 r_1^2 C_{A2}}{C_{A1}} + \frac{r_3 r_1^2 C_{A3}}{C_{A1}}} \tag{7}$$

Further rearrangement allows for the calculation of the concentrations by mass for each remaining particle size:

$$C_{M_2} = \frac{r_2^3}{r_2^3 + \frac{r_1 r_2^2 C_{A1}}{C_{A2}} + \frac{r_3 r_2^2 C_{A3}}{C_{A2}}} \tag{8}$$

$$C_{M_3} = \frac{r_3^3}{r_3^3 + \frac{r_1 r_3^2 C_{A1}}{C_{A3}} + \frac{r_2 r_3^2 C_{A2}}{C_{A3}}} \tag{9}$$

The relationships for particle concentration by mass Eqs. (7)–(9) can therefore be used to translate measurements of particle concentrations by area to concentrations by mass using known particle size radii for a tridisperse mixture.

Transparent box validation

A small-scale transparent box was built to image mixtures consisting of different proportions by mass (or volume) of the subject particle sizes to confirm the relationship derived above (Fig. 5a). Once each mixture was poured into the box, each side was imaged with a Sony DSC-RX10 II camera. Images were then cropped to 0.1 m widths and analyzed for particle size concentrations by area (e.g. Figure 5b). The mixture was then remixed, and the box refilled 5 times, resulting in 20 images of particle concentrations by area per mixture.

This process was conducted for three mixtures with 3:6:12 mm particle mass ratios of 1.5:1:0.5, 1:1:1, and 0.5:1:1.5, respectively. All calculations utilized the particle size radii measured by Coombs et al. (2020) rather than the nominal radii. Concentrations by area determined for each particle size are presented in Fig. 6 as a box and whiskers plot, along with the actual concentrations of particle size marked as black dashed lines. These concentrations were translated to concentrations by mass using Eqs. (7)–(9) for each respective particle size and mixture.

For each mixture tested, the same trends in conversion between area, volume, and mass are observed for each particle size (Fig. 6).

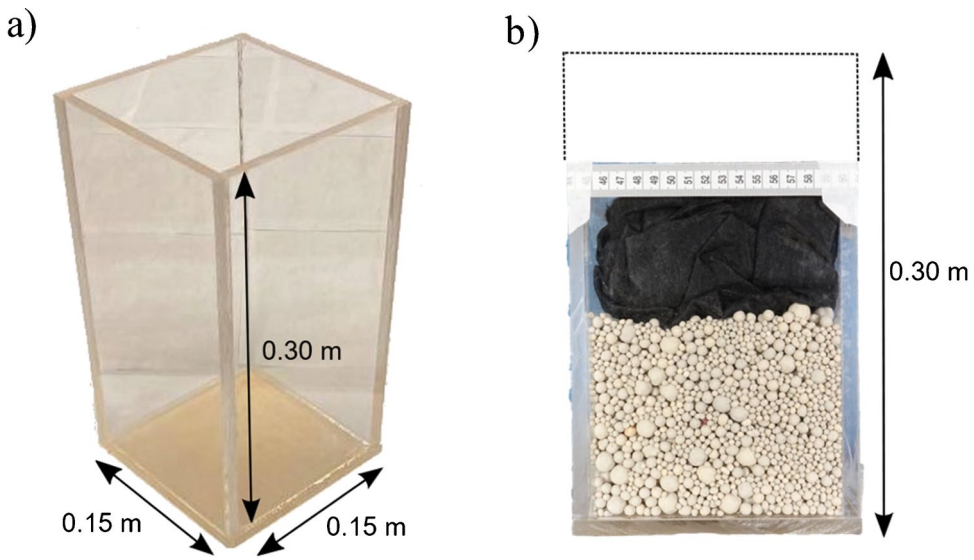

Fig. 5 Dimensioned **a** transparent glass box used for concentration by area measurements and **b** sample image captured

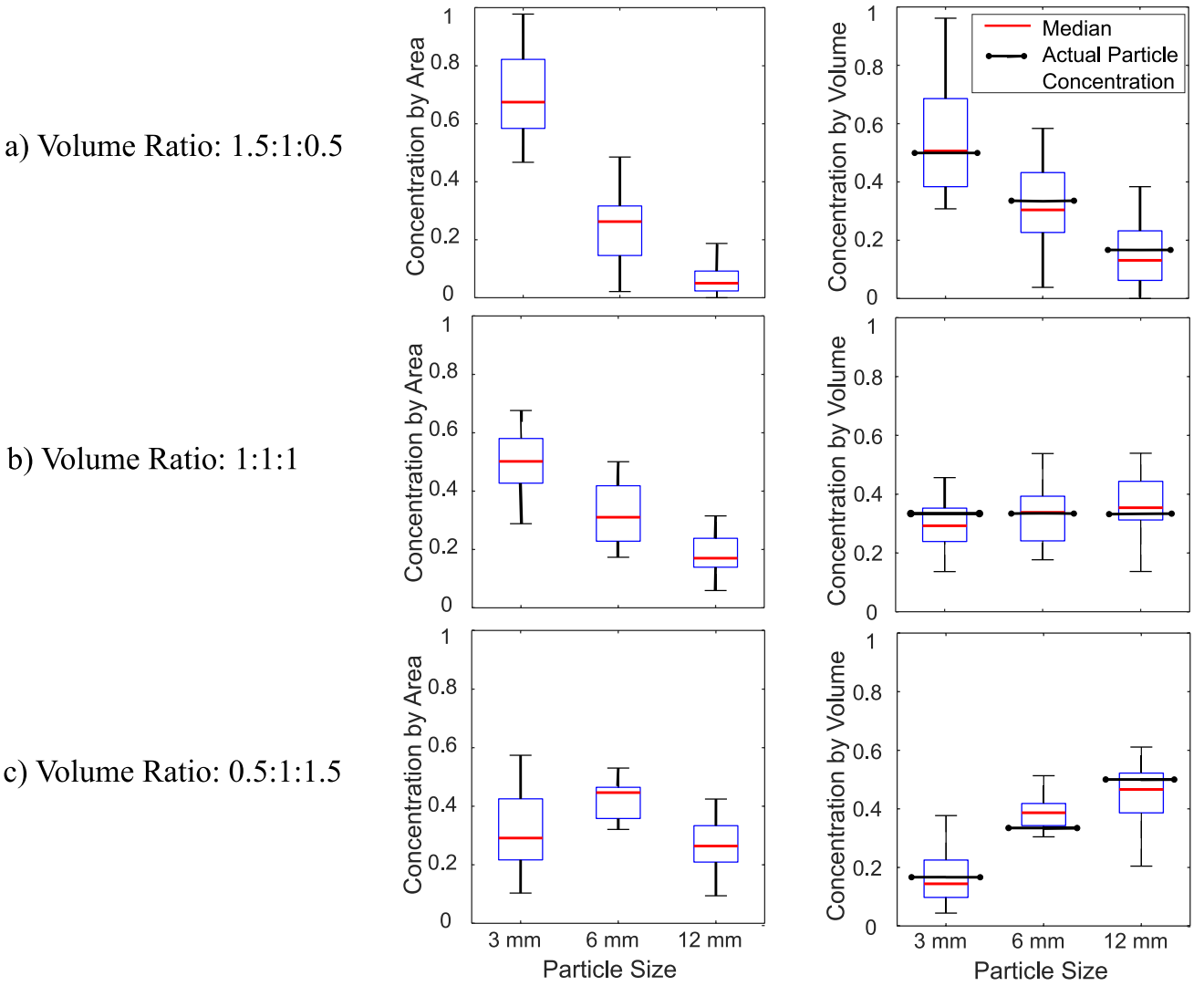

Fig. 6 Box and whiskers plots of experimentally obtained particle size concentrations by area translated to particle size concentrations by solid volume, using the empirically determined volume to area relationship, for the conducted transparent box experiments. The actual particle size concentrations by mass/volume used in the experiments are marked on the concentration by volume box and whiskers plot for the respective particle size, 3:6:12 mm, volume ratios, **a**, **b**, and **c**

The concentrations by area of the 3 mm particles present higher than their corresponding concentrations by mass, while those of the 6 mm particles present similar values, and those of the 12 mm particles present lower values. These trends are as expected given the different scaling that different radii are subject to in the calculation of area and mass/solid volume. Additionally, for each mixture tested, good agreement is seen between calculated median particle size concentrations by mass and the physically measured particle size concentrations by mass of the mixtures studied (Fig. 6). This visual agreement indicates that the relationship outlined in Eqs. (7)–(9) reasonably captures how concentrations by area convert to concentrations by mass in spherical tridisperse mixtures.

In addition to the validation of the theoretical relationships for particle size concentrations, these tests demonstrate the value in replicate testing in measurements of segregation. Significant scatter was seen in the transparent box results (Fig. 6) which is representative of segregation that occurs during the filling process and the statistical likelihood that a representative distribution of particles is being captured in analyzed images. Sample windows were designed to be 0.1 m wide by 0.2 m high to match the typical size of those from the experimental landslide deposits. Therefore, the scatter observed may be considered to be representative of the larger experiments.

For this study's subject experiments, utilizing a material source volume of 0.6 m^3 with a mass of approximately 915 kg, it is not possible to execute twenty replicate tests to obtain the same number of replicate data points as the transparent box experiments. From a practical perspective, a minimum of four replicate tests for each internal deposit sampling method attempted was chosen at the outset of the experimental design. This decision was based on the assumption that a significant portion of the scatter observed in the box tests was due to segregation occurring during the filling

process. In the remainder of the paper, particle size concentrations are presented both in terms of concentrations by area to enable visual comparisons with the captured images and as particle concentrations by mass to evaluate the correspondence of each method to the concentrations of the original source volume.

Landslide and landslide deposit observations

Landslide characteristics

A typical experiment using the flume is shown in the video included as supplementary information. The characteristics of the granular flow developed in the landslide segregation experiments are presented in Fig. 7 in terms of a time history of flow height and velocity at an observation point (Fig. 3), for three replicate tests. Figure 7a shows individual flow behaviour using coloured lines, while Fig. 7b uses the same legend markers across all three replicates to identify trends. Overall, each replicate test yielded similar flow height and velocity data, demonstrating consistent behaviour.

Over the duration of flow, the height of flow peaked at around 80 mm as the initial dilated flow front passed the observation point, dropped to between 50 and 65 mm for approximately 1.5 s as a coherent flow body then dropped again to approximately 40 mm and continued to decrease as a thinning flow body (Fig. 7a). Additionally, velocity measurements were taken for the top of flow, average flow, and base of flow (basal slip velocity) (Fig. 7b). All measured velocities were initially high at the flow front of saltating and collisional particles. After the initial front passed, a more coherent body of material passed the observation point, and the velocity measurements diverged. Top of flow velocities remained higher than the average flow or basal slip flow velocities due to the profile of shear within the flow. Large particles preferentially migrating to the top of the flow therefore are also preferentially delivered to the front of the flow due to the higher velocity in this region. As expected from Johnson et al. (2012), Iverson (2014), and Turnbull et al. (2015), these observed initially tall fast flows which slow and thin towards their tail ends match the behaviour of natural debris flows, which in general have thick coarse fronts followed by thinning tails. These results also illustrate how longitudinal segregation occurs, with faster top of flow velocities and slower basal slip velocities developing over the flow duration.

External landslide deposit characteristics

Landslide deposits were analyzed to determine particle sizes and locations through the transparent flume sidewall. This information is visually presented in Fig. 8 for one replicate with particle markers represented by their respective diameters and located in their calculated position within the deposits relative to the incline, R(m). As anticipated in the longitudinal direction, the large 12 mm particles dominate the front, and the small 3 mm particles dominate the back of the deposit, with medium 6 mm particles scattered throughout.

Figure 9 quantifies the data presented in Fig. 8 across all six replicates. The trend of a coarse-grained front, transition zone, and fine-grained tail corresponds to a typical debris flow deposit morphology. The average total runout distance of a deposit R_{max} for the six replicate tests was 2.08 m. Distance from the flume incline, R(m), was normalized to R_{max} to examine vertical segregation using three 0.3 m sections of interest, labelled in Fig. 9. These were selected along the runout distance to assess vertical segregation, with each position corresponding to different longitudinal zones of segregation (e.g. the coarse-grained front, transition zone, and fine-grained tail of the deposit).

Figure 10 presents vertical concentration by area for these sections in terms of normalized height, y/h, where y is the height of a vertical bin and h is the height of the deposit. Connected points represent data from individual tests. Small particles dominate throughout the vertical range at the tail end of the deposit (Fig. 10a), while large particles dominate throughout at the front (Fig. 10c). However,

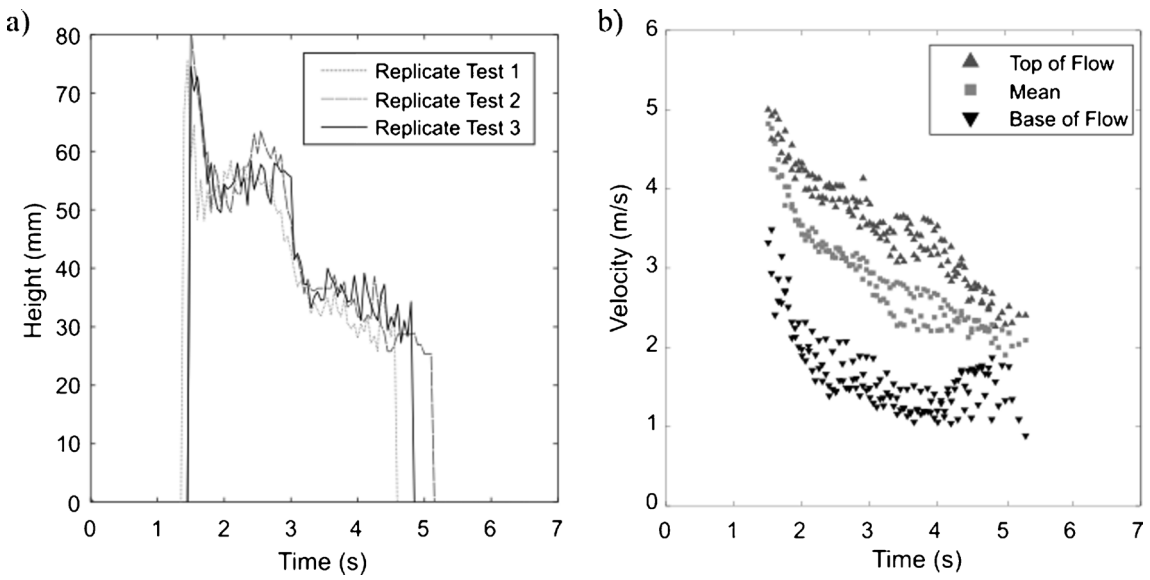

Fig. 7 Graphs of **a** height of flow and **b** particle flow velocity, versus time since release box door opening taken from a fixed observation point for 3 replicate tests

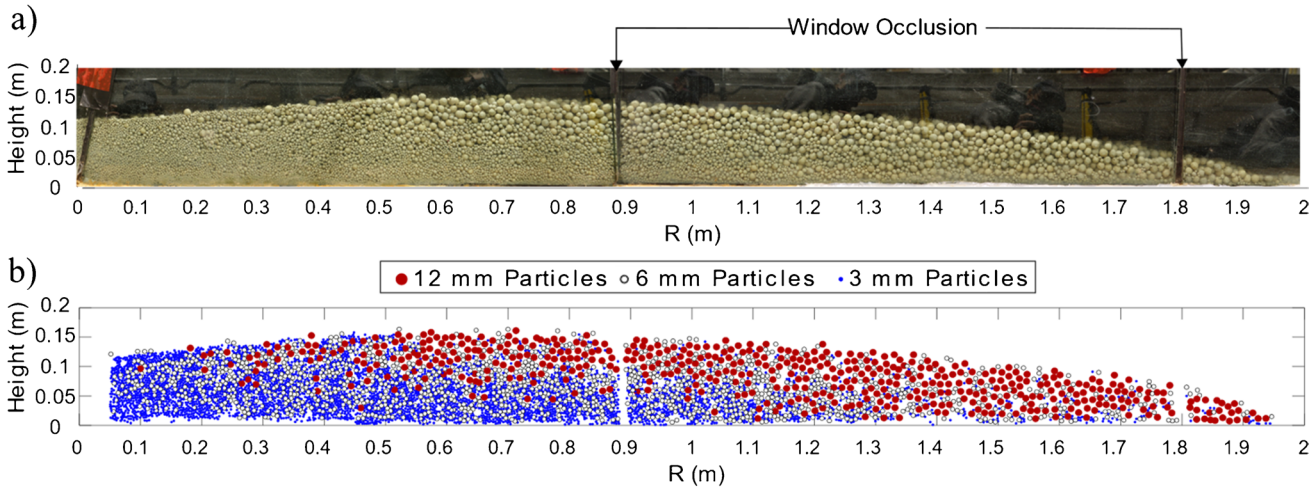

Fig. 8 Sample **a** external sidewall view of a deposit imaged and **b** schematic cross section reproduced using particle size analysis results from deposit images. The diameter of the particle size markers corresponds to the difference in diameter between the respective particle sizes

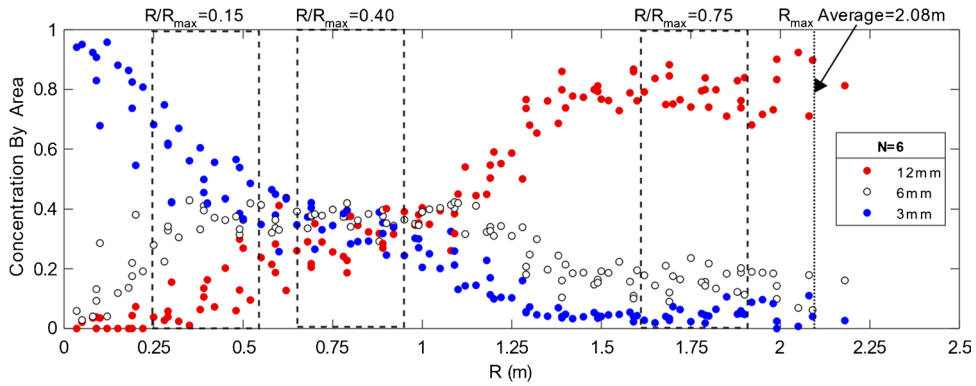

Fig. 9 Collective raw longitudinal particle distribution results of six replicate tests as seen from external flume sidewall with points of interest marked

in the middle section or transition zone at an R/R_{max} of 0.4, in which particle size concentrations by area are evenly distributed longitudinally, very clear vertical segregation is seen (Fig. 10b). Large particles are focused at the top of the deposit, small particles at the bottom, and medium-sized particles are consistent in concentration throughout the deposit height.

This data indicates that strong vertical segregation is present in the deposit where particle size concentrations are relatively evenly distributed. However, towards the front or tail of the deposit, where longitudinal segregation has caused one particle size to dominate, vertical segregation is far less apparent.

Internal longitudinal segregation observations

Several internal deposit sampling methods were trialled to observe segregation trends along the centerline of deposits. Placing a stationary internal plane, inserting a plane horizontally, and inserting a plane horizontally in increments were employed for the internal cross-sectioning of, respectively, four, five, and four replicate test deposits.

Particle size concentrations by area, plotted with respect to normalized deposit runout distance, are presented in Fig. 11 for the external sidewall observations and internal deposit observations obtained through the stationary plane and horizontal plane insertion methods. In these figures, the boundaries of the transition zone, the points at which the coarse grain front ends and the fine-grained tail of the deposit begins, were visually assessed. The point at which particle size concentrations by area first converged, extending from the front of the deposit, was considered to be the coarse-grained front transition zone boundary. The point at which these particle size concentrations by area next diverged, extending from the front transition zone boundary, was considered the fine grain tail transition zone boundary.

Along the external flume sidewall, very clear segregation is seen in the longitudinal direction (Fig. 11a). The transition zone boundaries were visually determined to be at R/R_{max} of 0.3 and 0.5, with particle size concentrations by area clearly diverging before and after these values. In comparison, the stationary plane method

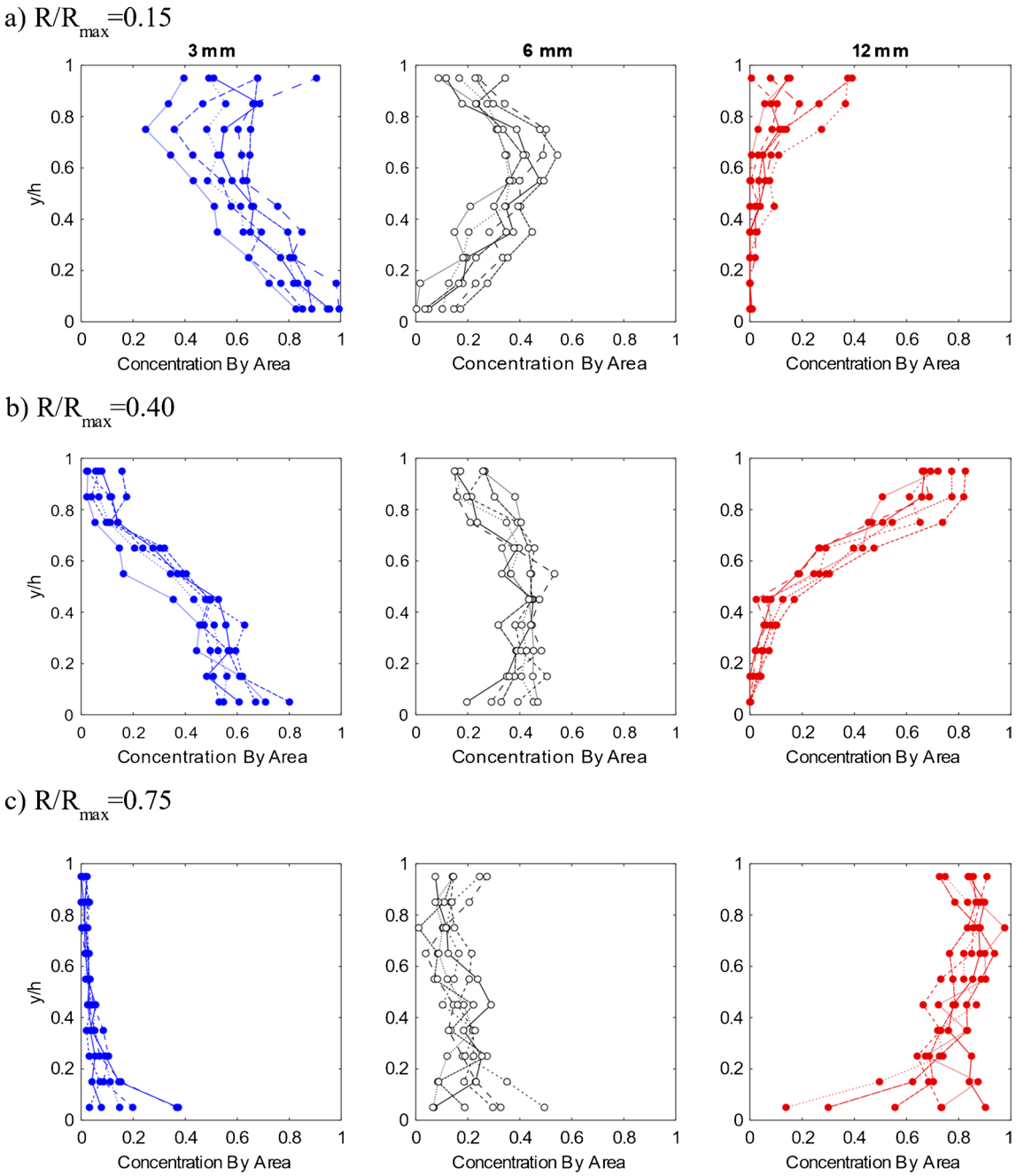

Fig. 10 Collective height normalized vertical particle distribution results of six (6) replicate tests taken at **a** $R/R_{max}=0.15$, **b** $R/R_{max}=0.40$, and **c** $R/R_{max}=0.75$, as seen from external sidewall. Connected markers represent data points from the same tests

also results in clear longitudinal segregation (Fig. 11b). However, longitudinal segregation observed by this internal method shows more consistent particle size concentrations outside of the transition zones compared to that seen from the external flume window. For example, the internal plane shows a constant concentration of 6 mm particles across the deposit, whereas along the external flume sidewall, a variation is seen. Additionally, the transition zone boundaries are located further towards the front of the deposit, at approximately R/R_{max} of 0.6 and 0.7, respectively, compared to the external sidewall.

Particles are subject to shear as they move along both the external flume sidewalls and the internal stationary plane at the base of the flume. During the entire duration of the flow, particles interacting with the sidewall of the flume are subject to shearing, which encourages segregation (Golick and Daniels 2009; May et al. 2010). In the case of the stationary internal plane, particles only interact with the plane in the runout section of the flume, 2.44 m maximum, which is a significantly shorter distance than the length travelled by the flow (approximately 11.5 m). This difference in shearing distance accounts for the shifted transition zone boundaries in the internal

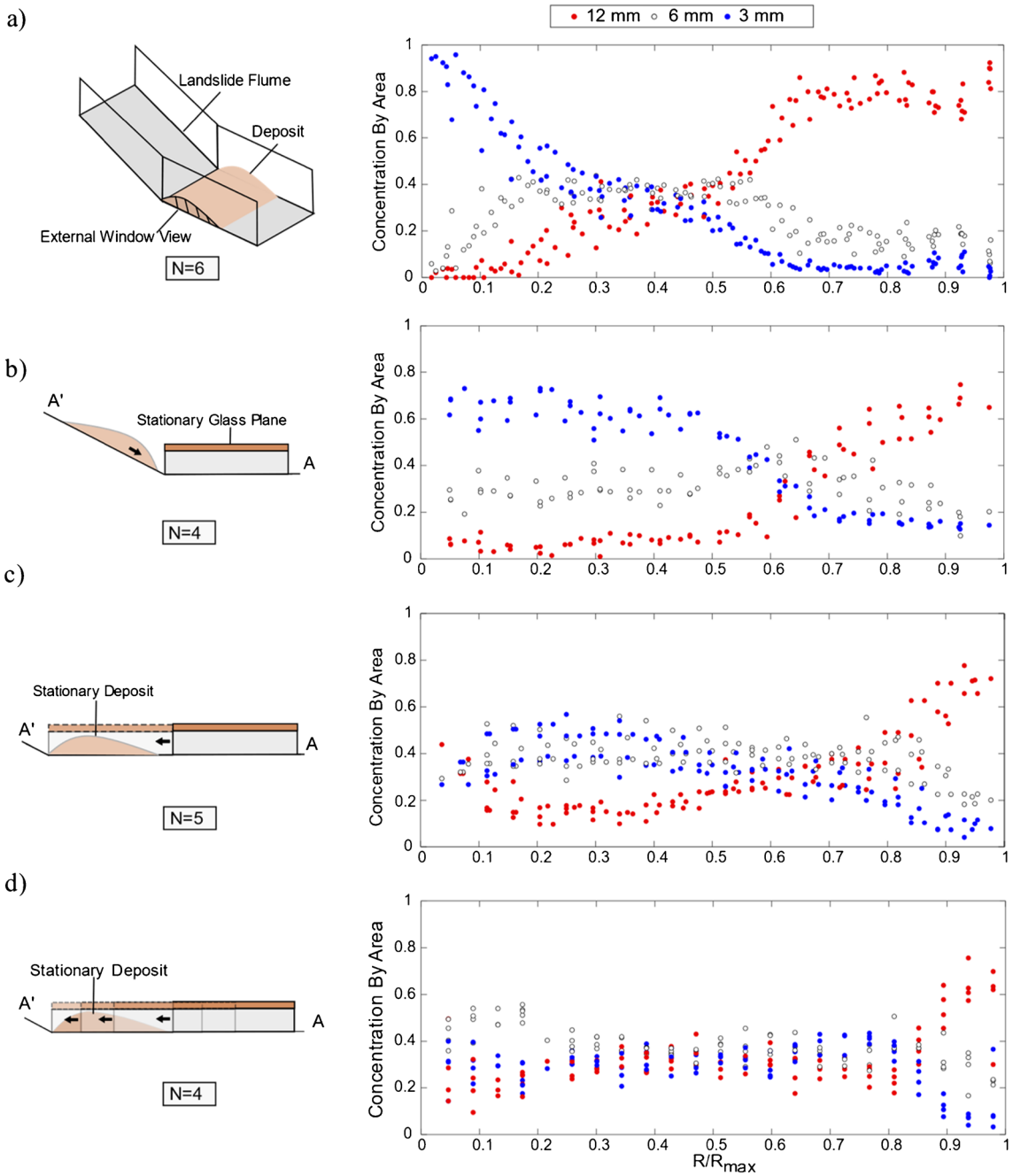

Fig. 11 Longitudinal particle distribution results as seen from **a** external sidewall, **b** internal cross section generated using stationary plane method, and internal cross section generated using horizontal insertion method post-test in either a **c** single push or **d** incremental push

stationary plane cross sections relative to those observed through the external flume sidewall.

Observations made using the horizontally inserted plane cross-sectioning method, Fig. 11c, differed significantly from the external sidewall observations. For this method, the internally observed coarse-grained front of the deposit, at R/R_{max} of 0.85 to 1, initially shows very clear segregation. However, the transition zone boundaries for the horizontally inserted plane tests occur at a R/R_{max} of 0.55 and 0.85, so that the front boundary of the transition zone is closer to the front of the deposit than seen in sidewall observations. Nonetheless, the transition zone extends further than that observed for the internal stationary plane method, indicating some discrepancy between the two.

Longitudinal particle size distribution results for four replica tests utilizing this incremental insertion method are presented in Fig. 11d. Similar to the results of the horizontal insertion method, the transition zone front boundary is close to the front of the deposit at an R/R_{max} of 0.85, but the transition zone extends further than that seen with the horizontal insertion method, to an R/R_{max} of 0.25. These results suggest that longitudinal segregation along the

centerline of the deposit is weakened. This weakened longitudinal segregation trend is also seen in the horizontal insertion method, in the form of an elongated transition zone; however, it is enhanced using the incremental horizontal insertion method.

The differences in outcomes between internal plane methods are of interest, such that it is not clear which produces a more reliable representation of an undisturbed deposit centerline. Therefore, an investigation on segregation induced by the shearing of a plane was undertaken to clarify the cause of this discrepancy.

Segregation induced by the shearing of a plane

The significance of segregation induced by the shearing of a plane was assessed through the analysis of 0.1 m wide images, of 0.1 m width, taken of a deposit in a fixed location as a horizontal plane was inserted (Fig. 12a). Images were captured for each 0.1 m of plane movement and analyzed for particle size concentrations by area. Sample images of the deposit from a fixed location are shown for 0.47 m, 1.27 m, and 2.07 m of plane movement across the deposited particles along with their corresponding vertical particle size distributions in Fig. 13. There is a significant height change in the deposit as the plane shears through it. This height change also corresponds to a drop in 3 mm and 6 mm particle concentrations by area and rise in 12 mm particle concentrations. There are several mechanisms at play here: the change in particle concentrations indicates an increase in vertical segregation as the plane shears through the particles; the height decrease corresponds to both contraction and out-of-plane movement of the particles. Smaller 3 mm particles are pushed into the body of the deposit during shearing, and larger 12 mm particles move towards the boundary, while overall the packing of material being disturbed becomes more efficient.

The change in overall particle size concentrations by area over 1.5 m of plane movement is presented in Fig. 12b. Initial particle size concentrations by area are relatively equal; however, with increased plane shearing, segregation becomes increasingly pronounced until approximately 1.27 m of shear has occurred after which point particle size concentrations by area remain relatively constant. This suggests that after a certain amount of shearing, particles will no longer rearrange as they are already in a fully segregated state.

Overall, this investigation demonstrated that the horizontally inserted plane method generated significantly more sample disturbance than initially assumed. The incremental horizontal plane insertion method limits shearing caused sample disturbance and therefore generates more reliable results. However, although limited, the incremental horizontal plane insertion method is still subject to shearing which generates sampling disturbance.

Visual comparison of external and internal landslide deposit characteristics

Representative deposit cross sections, highlighting particle normalized locations and sizes, generated from each cross-sectioning

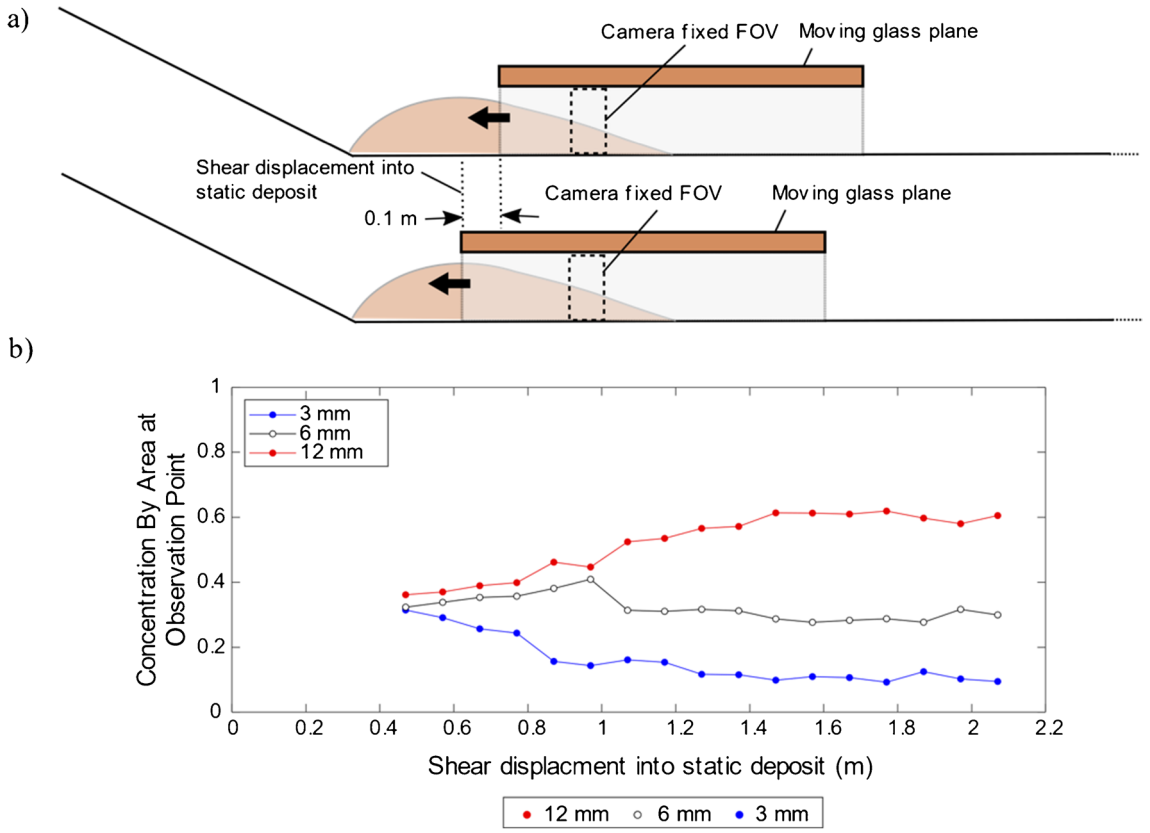

Fig. 12 Schematic of **a** shear investigation setup with a fixed camera field of view and moving glass plane (causing shear displacement) and graph of **b** particle size concentrations from fixed camera field of view as glass boundary plane is inserted in 0.1 m increments

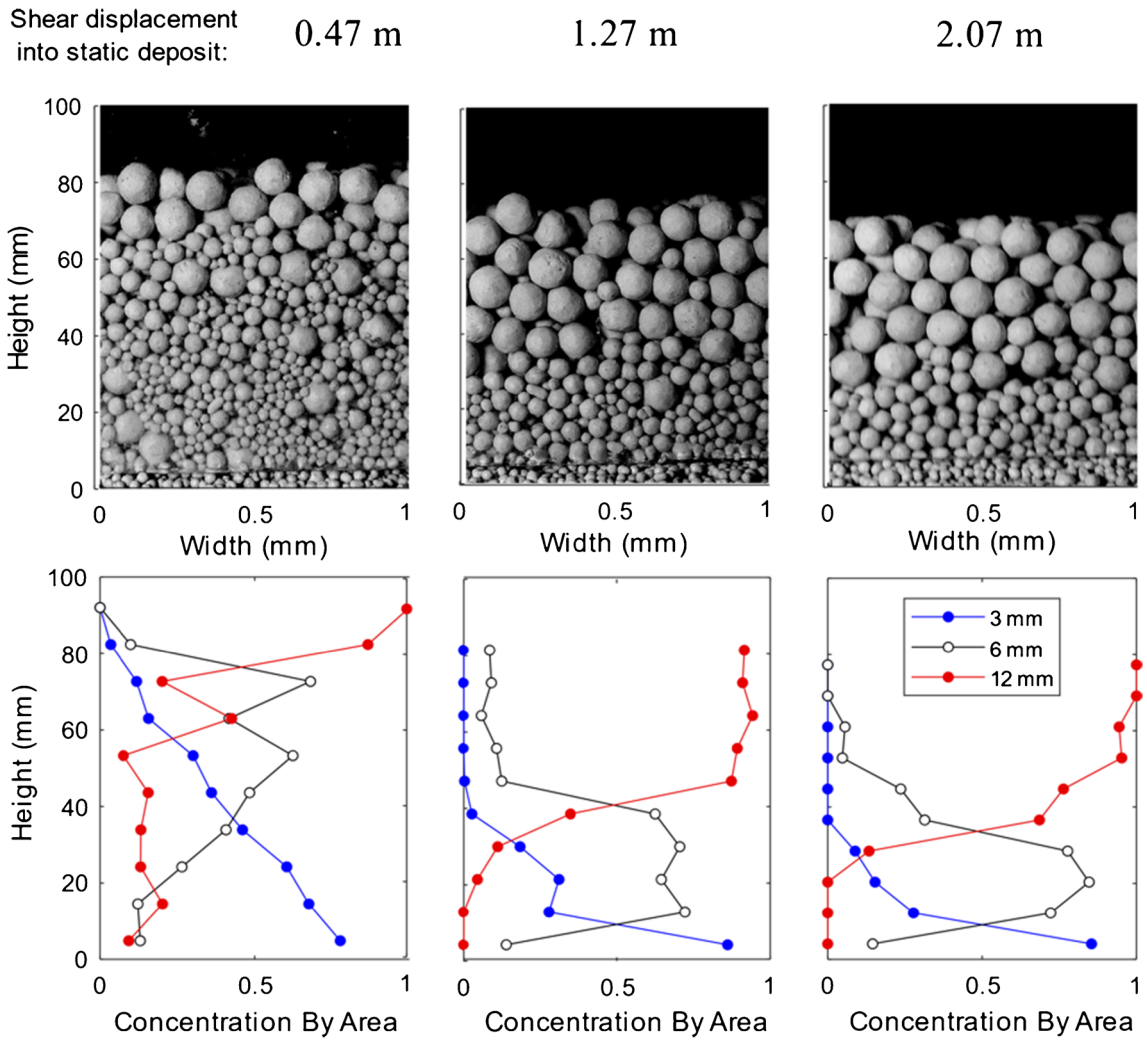

Fig. 13 Sample images, taken from a fixed position, and corresponding vertical particle size concentrations by area taken with a glass boundary plane inserted 0.47 m, 1.27 m, and 2.07 m into the deposit (shear displacement amounts). Note the bottom edge of the glass boundary plane is shown in the base of the sample images as the glass boundary plane is not perfectly flush with the base of the flume

method and external sidewall observations are presented in Fig. 14. It should be noted that the differences between these cross sections are attributed to the differences in the sampling methods used. The cross sections presented were chosen to be representative of all replicate tests performed using a particular sampling method. Height (H) is normalized to the max height (H_{max}) of the respective deposit.

The external sidewall cross section (Fig. 14a) shows particle size segregation in the longitudinal direction and an overall high presence of large, 12 mm, particles relative to that seen from the internal observations. The internal stationary plane cross-section (Fig. 14b) also shows segregation more dominantly in the longitudinal direction than the vertical; however, significantly fewer 12 mm particles are present in this internal cross section. The horizontal insertion and incremental horizontal insertion cross sections (Fig. 14c and d, respectively) both show significant vertical segregation and less prominent longitudinal segregation. The number of 12 mm particles in these cross sections more closely matches those within the internal stationary cross section.

When a flow is unconfined, coarse-grained lateral levees form due to particle segregation circulating coarse particles to the edges of flow, which also generate channelized flow through the center of the body (Johnson et al. 2012). These lateral levees are unable to form in the test deposits generated for this study due to sidewall confinement; however, the dominance of 12 mm particles in the external sidewall cross-section suggests that coarser particles are still being advected to flow edges. The internal stationary plane cross-section shows a similar effect occurring at the deposit front, but this effect is less prominent than that seen through the external sidewall. The internal stationary plane acts as a confining boundary for the flow body once it reaches the runout section of the flume. The effect of large particles circulating to this internal boundary is less significant than that seen with the external sidewall window as this boundary is only

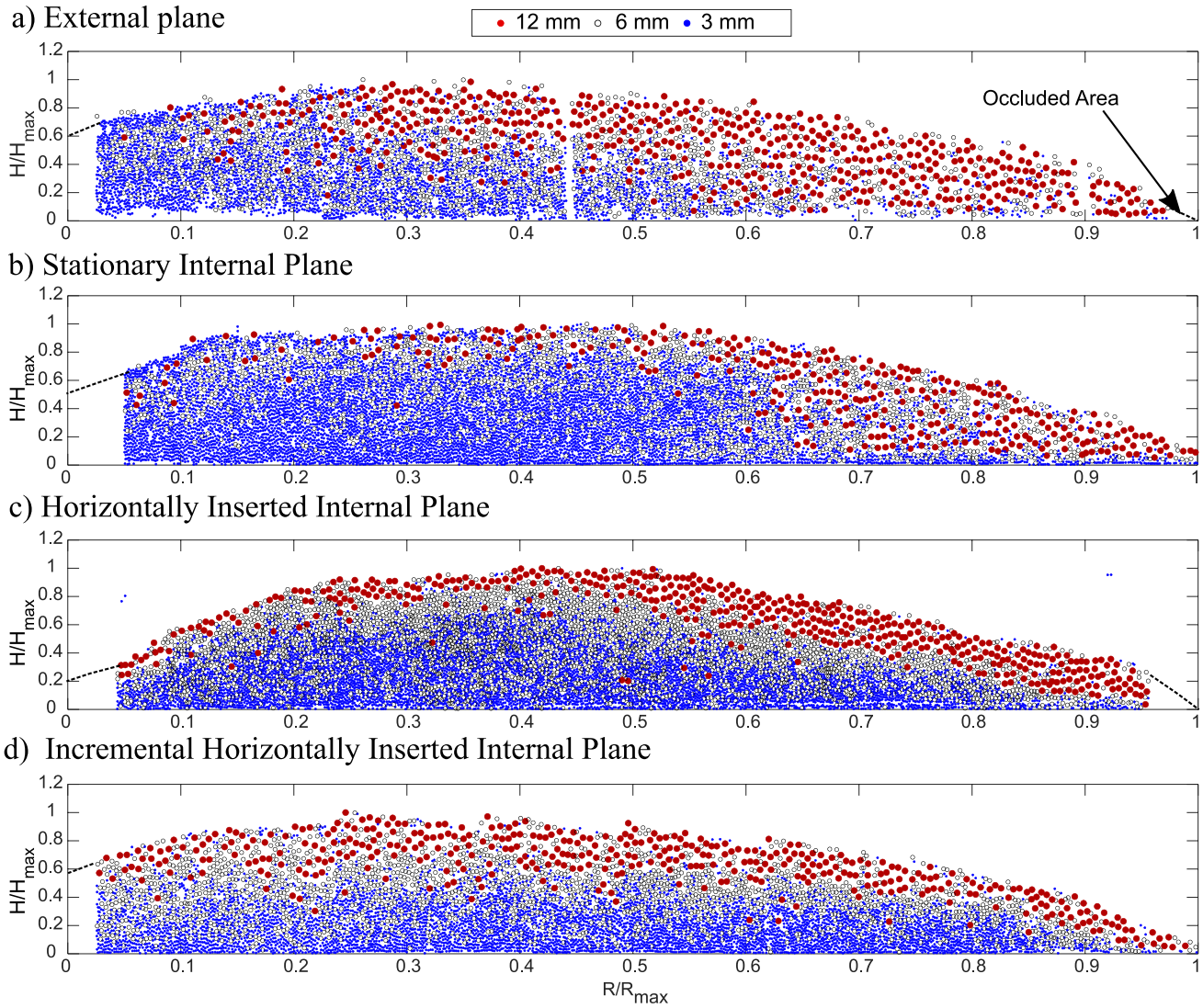

Fig. 14 Deposit sample cross-sections displaying particle locations and sizes for **a** external sidewall view of deposit and internal cross-sections produced using **b** stationary internal plane method, **c** horizontally inserted internal plane method, and **d** incremental horizontally inserted plane method

present through the small runout section of the flume, for 2.44 m maximum, so this effect has less distance over which to develop in the flow body.

The internal sampling methods attempted all provided results more similar to each other than those generated from sidewall observations. The results of the internal insertion cross-sectioning methods suggest the centerline of these flow deposits is more heavily segregated in the vertical than the longitudinal direction. This is in agreement with the quantitative assessments presented in Fig. 11c and d. The observations made using the incremental horizontal insertion method are more reliable than those made with the horizontal insertion method, as sample disturbance was much less. While vertical segregation is likely more exaggerated in deposit cross-sections generated using plane insertion methods, the horizontal incremental method minimizes the disturbance.

Segregation observations by mass

Concentration by area measurements is biased towards a higher presence of small particles due to the neglect of the three-dimensional aspect of particles. Concentrations by mass for each particle size, calculated from the empirical relationship defined by Eqs. (7)–(9) for representative deposits of each deposit cross-section type, are presented in normalized terms in the bar chart included in Fig. 15. The concentration by mass trends in this data are comparable to the visual area representations of each cross-section method presented in Fig. 14. As expected, these concentrations by mass show a large presence of 12 mm particles and significantly less of 3 mm particles in comparison to concentration by area information. Due to this, transition zone boundaries are located closer to the tail of the deposit than in corresponding quantified concentration by area observations.

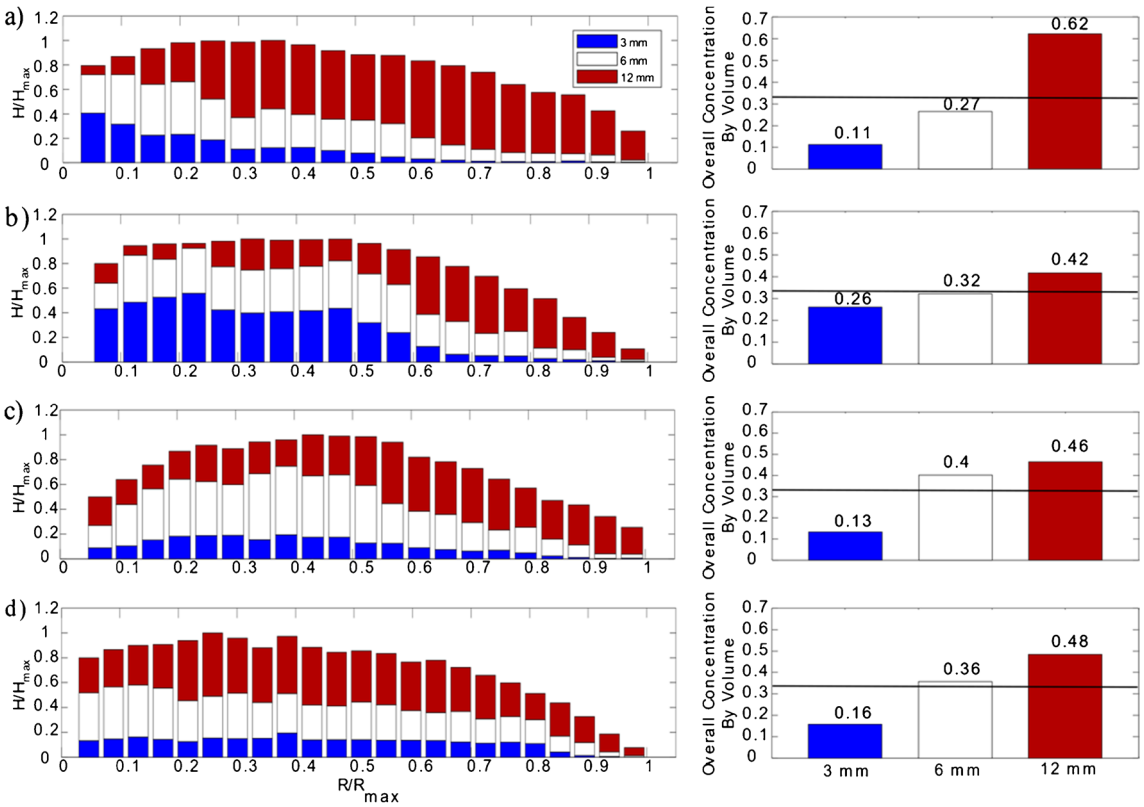

Fig. 15 Stacked bar chart of deposit concentrations by volume of each particle size for **a** external sidewall view of deposit and internal cross-sections produced using **b** stationary internal plane method, **c** horizontally inserted internal plane method, and **d** incremental horizontally inserted plane method. The height of each bar is representative of the height of the deposit at the respective R/R_{max} location. Bar charts of overall particle size concentrations by volume for each sampling method are shown to the right of the respective stacked bar charts with a black line marking the source volume concentration of each particle size, 0.33 concentration. The **b** stationary internal plane method best matches the initial source volume concentration of each particle size

The integration of the concentrations by mass throughout the entire measurement plane provides an opportunity to comment whether the concentrations by mass in this plane are representative of the known concentrations of the original source volume. These calculations have been performed for each sampling method and are presented in Fig. 15. In Fig. 15a, the longitudinal distribution of concentration by mass is shown as a stacked bar chart. If these values are summed, the total concentration of each particle size can be calculated. If a method is representative of the known concentration of the original source volume, the total concentration by mass/solid volume would be 0.33 for each of the 3, 6, and 12 mm particles. This integrated data indicates that the cross section generated along the external sidewall most significantly deviates from the original mixture. In contrast, the internal stationary plane method most closely represents that of the original source volume. It can be inferred that this method causes the least out-of-plane segregation of particles resulting from the measurement technique employed.

Conclusions

Flow structures in landslide deposits are important for the geomorphological interpretation of landslide mechanisms. Particle size segregation is a key characteristic that may occur during landslides, such as debris flows, rock avalanches, and debris avalanches: linking the physical manifestation of segregation in the field to that under controlled laboratory conditions is therefore important, given that numerical models of segregation are generally validated against such experiments. The critical question regarding quantification of segregation in laboratory flume experiments relates to whether visual observations of particle size distributions captured at a transparent external boundary are significantly different from internal measurements. A second question then arises as to whether sampling by the insertion of a transparent plane could introduce biases in the measurement of segregation.

As a first step to answering these questions, an analytical relationship was derived for tridisperse mixtures, as used in subsequent flume experiments, to enable the translation of sidewall concentrations calculated by area to concentrations by mass/solid volume. Small-scale experiments confirmed this relationship and emphasized the need for replicate tests to be performed to allow for statistical variability.

Nineteen replicate landslide flume tests using 0.6 m^3 of even sizes by mass of tridisperse particles revealed consistent overall flow behaviour, with initially fast and tall flow fronts followed by slowing and thinning flow tails. Replicate tests were used as a strategy to increase the accuracy of the quantification of the degree of particle size segregation.

Observations at the external sidewall of the flume in replicate tests showed very clear longitudinal segregation, with a coarse-grained front, transition zone, and finer-grained tail. Additionally, vertical segregation was shown to be prominent in the transition zone of the deposit from this sidewall data. Sets of replicate tests were then performed to explore three internal sampling strategies to quantify the differences in the distribution of particle sizes at the centre of the deposit and at the external transparent window.

Internal cross sections generated using the internal stationary plane method showed evidence of longitudinal segregation, however, these patterns did not match those seen from the external flume sidewall. Transition zone boundaries were observed to be closer to the deposit front than that seen from the sidewall, which is likely to be due to differences in boundary interaction length. Additionally, particle size concentrations by area were found to be more consistent into the tail of internal stationary plane deposits than at the sidewall.

The vertical insertion of a glass plane into a deposit could not be carried out in a controlled and consistent manner and therefore was not further investigated. The horizontal insertion of a thin glass plane into the centerline of a deposit produced a similar degree of segregation at the front of the deposit as that using the internal stationary plane method. However, past the initial front, longitudinal segregation is significantly less prominent. Incremental insertion of a plane into a deposit was found to cause significantly more disturbance than was expected, especially with respect to vertical particle rearrangement. Otherwise, results of this method more closely matched those seen from the horizontal insertion method than the stationary internal plane method. All internal deposit observation methods gave results that were more consistent to each other than the results taken from the external side wall. This further confirmed the need for the increased use of internal observations and decreased reliance on sidewall observations in relevant granular flow research.

The integration of the concentrations measured using different methods over the entire deposit enabled an assessment of whether results were representative of the original source volume. Results at the external sidewall showed the most significant variation from the original mixture, with a relatively large presence of the largest (12 mm) particles. The increased presence of large particles suggests that shear along the boundary causes large particles to be preferentially advected to the flow edges as would occur in natural unconfined debris flows. In contrast, the internal stationary plane method produced an overall concentration that most closely represented the original source volume. It can be inferred that this method causes the least amount of out-of-plane segregation of particles resulting from the measurement technique employed.

Overall, this work produced valuable data sets for future development of theoretical models and calibration of numerical models of segregation. Sidewall influence on particle size distribution was illustrated, internal deposit observation techniques were investigated, and the stationary internal plane method was deemed the most pragmatic approach for future work. Future work on granular flows should decrease reliance on external sidewall observations and place an emphasis on internal observations in order to further current understanding of segregation dynamics in granular flows.

Funding

Funding for this research was provided by the Natural Sciences and Engineering Research Council of Canada (NSERC) under the Discovery Grant program awarded to W.A. Take (RGPIN-2020–04077). J.M.N.T.G. was supported by a Royal Society Wolfson Research Merit Award (WM150058) and an EPSRC Established Career Fellowship (EP/M022447/1).

Data Availability

Data used in this research can be downloaded from the following data repository: Kimball, Julia; Bowman, E.T.; Gray, J.M.N.T.; Take, W. Andy, 2024, "Evaluation of Laboratory Methods to Quantify Particle Size Segregation Using Image Analysis in Landslide Flume Tests", https://doi.org/10.5683/SP3/13Z7WG, Borealis.

Declarations

Conflict of interest The authors declare no competing interests.

References

Barker T, Rauter M, Maguire ESF, Johnson CG, Gray JMNT (2021) Coupling rheology and segregation in granular flows. J Fluid Mech 909:A22. https://doi.org/10.1017/jfm.2020.973

Bullard GK, Mulligan RP, Carreira A, Take WA (2019a) Experimental analysis of tsunamis generated by the impact of landslides with high mobility. Coast Eng 152:103538

Bullard GK, Mulligan RP, Take WA (2019b) An enhanced framework to quantify the shape of impulse waves using asymmetry. J Geophys Res: Oceans 124(1):652–666

Bullard GK, Mulligan RP, Take WA (2023) Landslide tsunamis: exploring momentum transfer to waves generated by a range of materials with different mobility impacting water. Landslides 20(12):2619–2633

Bunte K, Abt SR (2001) Sampling surface and subsurface particle-size distributions in wadable gravel- and cobble-bed streams for analyses in sediment transport, hydraulics, and streambed monitoring. Gen. Tech. Rep. RMRS-GTR-74. Fort Collins, CO: US Department of Agriculture, Forest Service, Rocky Mountain Research Station, 428, 74

Coombs SP, Apostolov A, Take WA, Benoît J (2020) Mobility of dry granular flows of varying collisional activity quantified by smart rock sensors. Can Geotech J 57(10):1484–1496. https://doi.org/10.1139/cgj-2018-0278

Cúñez FD, Patel D, Glade RC (2024) How particle shape affects granular segregation in industrial and geophysical flows. Proc Natl Acad Sci 121(6):e2307061121

Cuttler MVW, Lowe RJ, Falter JL, Buscombe D (2017) Estimating the settling velocity of bioclastic sediment using common grain-size analysis techniques. Sedimentology 64(4):987–1004. https://doi.org/10.1111/sed.12338

Deng Z, Umbanhowar PB, Ottino JM, Lueptow RM (2018) Continuum modelling of segregating tridisperse granular chute flow. Proc R Soc A: Math Phys Eng Sci 474(2211). https://doi.org/10.1098/rspa.2017.0384

Diplas P, Sutherland AJ (1988) Sampling techniques for gravel sized sediments. J Hydraul Eng 114(5):484–501. https://doi.org/10.1061/(asce)0733-9429(1988)114:5(484)

Fan Y, Schlick CP, Umbanhowar PB, Ottino JM, Lueptow RM (2014) Modelling size segregation of granular materials: the roles of segregation, advection and diffusion. J Fluid Mech 741:252–279. https://doi.org/10.1017/jfm.2013.680

Gajjar P, Johnson CG, Carr J, Chrispeels K, Gray JMNT, Withers PJ (2021) Size segregation of irregular granular materials captured by

time-resolved 3D imaging. Sci Rep 11(1):8352. https://doi.org/10.1038/s41598-021-87280-1
Golick LA, Daniels KE (2009) Mixing and segregation rates in sheared granular materials. Phys Rev E 80(4):042301. https://doi.org/10.1103/PhysRevE.80.042301
Gollin D, Brevis W, Bowman ET, Shepley P (2017) Performance of PIV and PTV for granular flow measurements. Granular Matter, vol. 19 no. 3. Springer, Berlin Heidelberg, pp 1–16. https://doi.org/10.1007/s10035-017-0730-9
Graham DJ, Rollet A-J, Rice SP, Piégay H (2012) Conversions of surface grain-size samples collected and recorded using different procedures. J Hydraul Eng 138(10):839–849. https://doi.org/10.1061/(asce)hy.1943-7900.0000595
Gray JMNT (2018) Particle segregation in dense granular flows. Annu Rev Fluid Mech 50(1):407–433. https://doi.org/10.1146/annurev-fluid-122316-045201
Gray JMNT, Ancey C (2011) Multi-component particle-size segregation in shallow granular avalanches. J Fluid Mech 678:535–588. https://doi.org/10.1017/jfm.2011.138
Gray JMNT, Chugunov VA (2006) Particle-size segregation and diffusive remixing in shallow granular avalanches. J Fluid Mech. Queen's University. https://doi.org/10.1017/S0022112006002977
Gray JMNT, Thornton AR (2005) A theory for particle size segregation in shallow granular free-surface flows. Proc Royal Soc A: Math Phys Eng Sci 461(2057):1447–1473. https://doi.org/10.1098/rspa.2004.1420
Iverson RM (2014) Natural Hazards. Geol Today 30(1): 15–20. Wiley
Jiang YJ, Fan XY, Li TH, Xiao SY (2018) Influence of particle-size segregation on the impact of dry granular flow. Powder Technol 340:39–51. https://doi.org/10.1016/j.powtec.2018.09.014
Jing L, Kwok FCY, Zhao T, Zhou J (2018) Effect of particle size segregation in debris flow deposition: a preliminary study. In: Farid A, Chen H (eds) Proceedings of geoshanghai 2018 international conference: geoenvironment and geohazard. GSIC 2018. Springer, Singapore. https://doi.org/10.1007/978-981-13-0128-5
Johnson CG, Kokelaar BP, Iverson RM, Logan M, Lahusen RG, Gray JMNT (2012) Grain-size segregation and levee formation in geophysical mass flows. J Geophys Res Earth Surf 117(1):1–23. https://doi.org/10.1029/2011JF002185
Kokelaar BP, Graham RL, Gray JMNT, Vallance JW (2014) Fine-grained linings of leveed channels facilitate runout of granular flows. Earth Planet Sci Lett 385, 172-180. Elsevier B.V. https://doi.org/10.1016/j.epsl.2013.10.043
May LBH, Golick LA, Phillips KC, Shearer M, Daniels KE (2010) Shear-driven size segregation of granular materials: modeling and experiment. Phys Rev E 81(5):051301. https://doi.org/10.1103/PhysRevE.81.051301
Cheng YM, Fung WH, Li L, Li N (2019) Laboratory and field tests and distinct element analysis of dry granular flows and segregation processes. Nat Hazards Earth Syst Sci 19(1):181–199. https://doi.org/10.5194/nhess-19-181-2019
Sanvitale N, Bowman ET (2016) Using PIV to measure granular temperature in saturated unsteady polydisperse granular flows. Granular Matter 18(3): 1–12. Springer Berlin Heidelberg. https://doi.org/10.1007/s10035-016-0620-6
Sanvitale N, Bowman ET (2017) Visualization of dominant stress-transfer mechanisms in experimental debris flows of different particle-size distribution. Can Geotech J 54(2):258–269. https://doi.org/10.1139/cgj-2015-0532
Savage SB, Lun CKK (1988) Particle size segregation in inclined chute flow of dry cohesionless granular solids. J Fluid Mech 189:311–335. https://doi.org/10.1017/S002211208800103X
Schlick CP, Isner AB, Freireich BJ, Fan Y, Umbanhowar PB, Ottino JM, Lueptow RM (2016) A continuum approach for predicting segregation in flowing polydisperse granular materials. J Fluid Mech 797:95–109. https://doi.org/10.1017/jfm.2016.260
Takehara K, Etoh T (1999) A study on particle identification in PTV - particle mask correlation method. J Visualization 1(3):313–323. https://doi.org/10.1007/BF03181412
Taylor-Noonan AM, Gollin D, Bowman ET, Take WA (2021) The influence of image analysis methodology on the calculation of granular temperature for granular flows. Granular Matter 23(4):1–17
Taylor-Noonan AM, Bowman ET, McArdell BW, Kaitna R, McElwaine JN, Take WA (2022) Influence of pore fluid on grain-scale interactions and mobility of granular flows of differing volume. J Geophys Res: Earth Surface 127(12):e2022JF006622
Trewhela T, Ancey C, Gray JMNT (2021) An experimental scaling law for particle-size segregation in dense granular flows. J Fluid Mech 916:1–37. https://doi.org/10.1017/jfm.2021.227
Turnbull B, Bowman ET, McElwaine JN (2015) Debris flows: experiments and modelling. Comptes Rendus Physique 16(1): 86–96. Elsevier Masson SAS. https://doi.org/10.1016/j.crhy.2014.11.006
van der Vaart K, Gajjar P, Epely-Chauvin G, Andreini N, Gray JMNT, Ancey C (2015) Underlying asymmetry within particle size segregation. Phys Rev Lett 114(23):1–5. https://doi.org/10.1103/PhysRevLett.114.238001
van der Vaart K, Thornton AR, Johnson CG, Weinhart T, Jing L, Gajjar P, Gray JMNT, Ancey C (2018) Breaking size-segregation waves and mobility feedback in dense granular avalanches. Granular Matter 20(3): 1–18. Springer Berlin Heidelberg. https://doi.org/10.1007/s10035-018-0818-x
Viroulet S, Baker JL, Rocha FM, Johnson CG, Kokelaar BP, Gray JMNT (2018) The kinematics of bidisperse granular roll waves. J Fluid Mech 848:836–875. https://doi.org/10.1017/jfm.2018.348
Wiederseiner S, Andreini N, Épely-Chauvin G, Moser G, Monnereau M, Gray JMNT, Ancey C (2011) Experimental investigation into segregating granular flows down chutes. Phys Fluids 23(1). https://doi.org/10.1063/1.3536658

Supplementary Information The online version contains supplementary material available at https://doi.org/10.1007/s10346-024-02375-w.

J. M. Kimball
Department of Civil Engineering, Queen's University, Kingston, ON, Canada

J. M. Kimball
Email: julia.kimball@queensu.ca

E. T. Bowman
Department of Civil and Structural Engineering, University of Sheffield, Sheffield S1 3JD, UK

E. T. Bowman
Email: e.bowman@sheffield.ac.uk

J. M. N. T. Gray
Department of Mathematics and Manchester Centre for Nonlinear Dynamics, University of Manchester, Manchester M13 9PL, UK

J. M. N. T. Gray
Email: nico.gray@manchester.ac.uk

W. A. Take (✉)
Canada Research Chair in Geotechnical Engineering, Department of Civil Engineering, Queen's University, Kingston, ON, Canada

W. A. Take
Email: andy.take@queensu.ca